A tri-band and miniaturized planar antenna based on countersink and defected ground structure techniques

Pierre Moukala Mpele, Franck Moukanda Mbango, Dominic B. O. Konditi, Fabien Ndagijimana

Received: Added at production | Revised: Added at production | Accepted: Added at production
DOI: xxx/xxxx

RESEARCH ARTICLE

A tri-band and miniaturized planar antenna based on countersink and defected ground structure techniques

Pierre Moukala Mpele*[1] | Franck Moukanda Mbango[2] | Dominic B.O Konditi[3] | Fabien Ndagijimana[4]

[1]Department of Electrical Engineering, Pan African University Institute for Basic Sciences Technology and Innovation, Nairobi, Kenya.

[2]Faculty of Sciences and Techniques, Electrical and Electronics Engineering Laboratory, Marien Ngouabi University, Brazzaville, Republic of the Congo

[3]School of Electrical and Electronic Engineering, Technical University of Kenya, Nairobi, Kenya

[4]Department of Electrical Engineering, Université Grenoble Alpes, CNRS, Grenoble INP, G2ELab, 38400 Saint-Martin d'Hères, France.

Correspondence
*Pierre Moulala Mpele,
Department of Electrical Engineering, Pan African University Institute for Basic Sciences Technology and Innovation, Nairobi, Kenya.
Email: pm.mpele@gmail.com

Abstract

In this paper, a compact planar heart-shaped antenna based on countersink and partial ground plane techniques is proposed to operate as a multiband device for modern wireless systems. With a surface area of 28.5 mm^2, the countersink technique has been developed to achieve high electromagnetic antenna performance. The countersink technique consists of a particular multilayer configuration that uses two distinct materials where one of them with a radiating element on its top is placed inside another. In this paper, a 508 µm thick Rogers RO4350B with a radiating patch designed on its top is thermally embedded into a 1.524 mm thick FR4 HTG-175. The slits are used to get multiband behavior, and their combination with the defected ground structure results in about 79.58% reduction in resonant frequency compared to the conventional antenna. A mathematical model is developed to predict the resonant frequency of the proposed antenna configuration. After modeling the heart-shaped antenna with an electromagnetic simulator, its prototype was manufactured and validated through experimental measurements. The countersink technique considerably improved the antenna's performance compared to the use of a single layer technology for the same antenna configuration. The return loss read from -10 dB shows that the proposed antenna covers multiple modern wireless applications, including LTE bands, 5G, WLAN, WiMAX, and Unlicensed National Information Infrastructure (UNII) radio bands. Furthermore, the antenna operates as narrowband and wideband simultaneously on its lower / middle and upper operating frequency bands. A close agreement is found between simulated and measured results across all the frequency bands.

KEYWORDS

Heart-shaped antenna, countersink, monopole, miniature antenna, multiband.

1 | INTRODUCTION

The fifth generation of mobile technologies (5G) is expected to connect people, objects, data, applications, transportation systems, and cities in smart grid communication environments[1]. At the same time, it will integrate and coexist with various existing services such as GPS, GSM, UMTS, Bluetooth, WLAN, WiMAX, 4G / LTE and more other wireless applications. In this context, multiple antennas can be used to cover different applications mentioned above. However, integrating several antennas into a single device is becoming more challenging due

Received: Added at production | Revised: Added at production | Accepted: Added at production
DOI: xxx/xxxx

to the space limitation of wireless mobile terminals [2]. So, compact and multiband antenna design has become very demanding [3].

Owing to their advantages of being low profile, lightweight, easy and low cost of fabrication, ease of integration within an environment of microwave circuit, planar monopole antennas with various structures are very popular in multiband applications [3]. Recently, multiple works on WLAN, WiMAX, 4G/LTE and 5G antennas using different methods have been reported in the literature. Material loading with very high permittivity dielectric, shorting and folding, reshaping or introducing slots, modification of the ground plane, and the use of metamaterials are among the techniques used for antenna miniaturization and multiband [4]. In Reference [5], a low profile multiband meander antenna was presented for LTE/WiMAX/WLAN and INSAT-C applications. The antenna has a size of 40×40×1.6 mm^3 and exhibits narrow bandwidths (70 and 90 MHz) in its first and second frequency bands. In Reference [6], the miniaturization of a 10 × 6 mm^2 rectangular patch antenna has been achieved with an inverted 'L' shaped ground plane for 5.2–5.8 GHz WLAN applications. A similar technique was used in Reference [7] to reduce the antenna size up to 86.72%. In Reference [8], a 30×20×0.8 mm^3 triband planar monopole antenna for WLAN and WiMAX operations has been designed and investigated. The multiband characteristic was achieved using a toothbrush-shaped patch, a meander line, and an inverted U-shaped patch, which resulted in three resonance frequencies.

Moreover, the defected ground structure (DGS) is one of the most significant techniques for achieving antenna compactness in terms of size or resonant frequency [9]. With the DGS and parasitic patch technique's help, a compact broadband antenna for LTE/WLAN/WiMAX applications has been proposed in Reference [10]. The antenna was designed on a 1.6 mm-thick square F4B substrate with a footprint of 30×30 mm^2. In reference [11], a 42.5×42.5×1.6 mm^3 compact circularly polarized slotted gap coupled semi-circular patch antenna for WLAN/WiMAX bands and other wireless applications. The antenna bandwidth improvement with better impedance matching have been achieved by etching slots on the patch and in the ground plane. In Reference [12], a triangular planar monopole antenna fed by fed by a microstrip gradient line has been proposed. With an overall size of 30×17×1.6 mm^3, the desired performance has been achieved using a partial ground plane along with an inverted-F shape and a 90º rotated counter-clockwise M-shaped structure. In reference [13], a multi-frequency antenna fabricated using FR-4 substrate with dimensions of 56×44×1.6 mm^3 is presented. An inverted T-shaped stub and two E-shaped stubs are used to generate multiple frequency bands, enabling the antenna to cover 4G LTE, WiMAX, WLAN, and S/C/X-band applications. A compact triband slotted printed monopole antenna for WLAN and WiMAX applications showing omnidirectional radiation pattern was presented in [14]. The physical size of the antenna is 27.5×20 mm^2. The triple-band operations and the desired antenna performance have been achieved by using an inverted L slot, Pi-shaped slot and a truncated square patch at its left corner.

Miniaturization can be defined as lowering the antenna's resonance frequency without changing its size [15]. At the same time, it is an art of compromise between radiation efficiency, gain, and bandwidth [14]**.** As planar antennas are miniaturized, various approaches and techniques are employed to maintain or enhance their performances. These techniques include the DGS, parasitic elements [16], air gap, slits, slots, metamaterial/metasurface, shorting pin [17,18], frequency-selective surface, electromagnetic band gap (EBG), meander line [19], and multilayered substrates. In most recent antenna designs, each technique's benefit is exploited and combined with others to get the desired results. For instance, in Reference [20], the antenna impedance matching and return loss have been improved using the defected ground structure through two F-shaped slots etched in the ground plane. In Reference [21], triple layers and double U-shaped slots have been used to achieve the multiband behavior and antenna bandwidth enhancement.

The size of the antenna's radiating element strongly affects its radiation efficiency and bandwidth [22]. Wider the bandwidth, larger is the size of the antenna [23]. This trade-off relationship between antenna size and bandwidth can reduce by using multiple layer substrates of different materials [24]. In Reference [25], a multilayer substrate configuration involving silicon/glass/silicon has been used to improve the far-field antenna parameter, including gain, directivity, and radiation efficiency. However, one of the drawbacks of the conventional multilayer configurations is the increased height, which is not desirable for conformal applications [26].

Received: Added at production | Revised: Added at production | Accepted: Added at production
DOI: xxx/xxxx

In this paper, a particular multilayer configuration is employed to improve antenna performance. Contrary to the conventional multiple substrate configuration, this paper investigates a miniature triband planar monopole antenna configuration where a Rogers RO4350B is embedded into FR4 HTG-175, leading to the countersink technique. A comprehensive design procedure is provided, and a mathematical model is developed to predict the resonant frequency of the antenna structure. The proposed triband heart-shaped planar monopole antenna (HPMA) covers several wireless communications applications such as Weather Radar, WLAN, WiMAX, 4G Long-Term Evolution (LTE), UNII radio bands, and 5G applications with a comprehensive design procedure. The HPMA design details and process are first presented, while the simulated and measured results are discussed later before highlighting the advantages and disadvantages of the configuration.

2 | ANTENNA CONFIGURATION

The geometry of the proposed antenna is presented in Figure 1. The top surface consists of a radiating patch made of two circular parts and a 45° rotated square. This yields a heart-shaped patch geometry fed by a microstrip feed line. The square's edge has been selected to be twice the circular part radius (Figure 1(b)). The antenna has an overall size of 15×12.5×1.524 mm^3. The structure is based on the countersink technique (CT) and the DGS, as shown in Figure 1. A single-sided Rogers RO4350B is thermally embedded into a double-sided FR4 HTG175 to provide a particular multilayer configuration. All the design parameters are listed in Table 1 below.

Table 1 Antenna design parameters

Parameter	**Value (mm)**	**Parameter**	**Value (mm)**
L_S	15	a_3	1
W_S	12.5	p	4.422
L	6.242	t	0.035
W	6.828	L_g	2.5
a	2	W_f	0.5
a_1	1.67	L_{RO}	6.085
a_2	1.25	W_{RO}	7
h_1	1.524	h_2	0.508

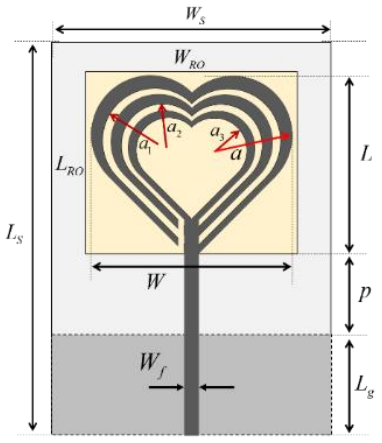

(a)

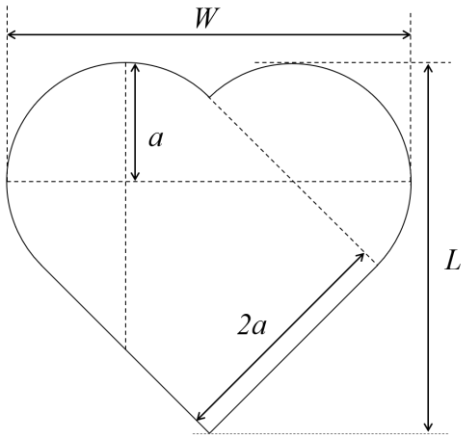

(b)

Received: Added at production | Revised: Added at production | Accepted: Added at production
DOI: xxx/xxxx

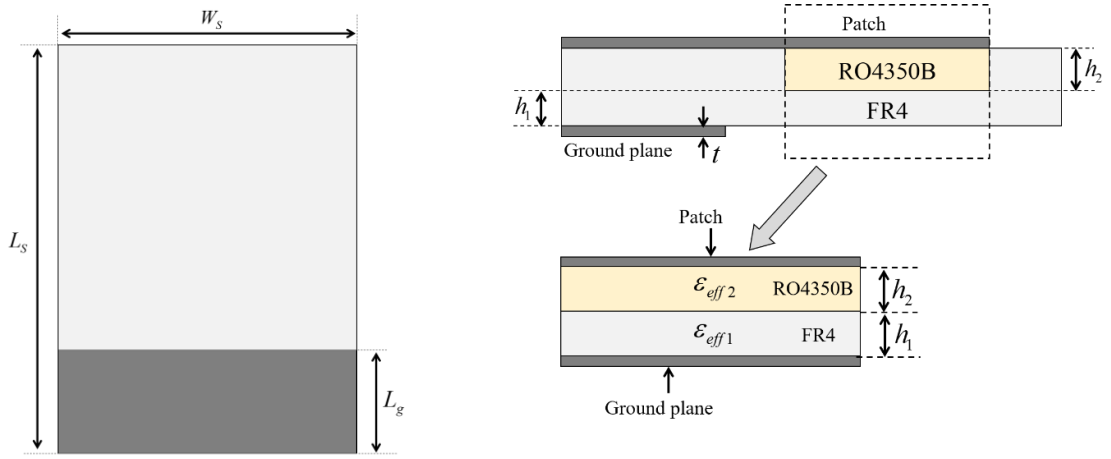

Figure 1 Proposed Antenna geometry. (a) top view; (b) heart-shaped configuration; (c) bottom view; (d) side view

The thickness of the copper cladding top and bottom used in the CT mentioned above is 35 μm. To reach the goal, current paths are created through slits etched on the radiating element illustrated in Figure 1(b), whereby every corresponding resonant paths' length Li is close to quarter-wavelength at its fundamental resonant frequency.

$$L_i = 10.283 a_i \text{ , } i=1,2,3 \tag{1}$$

$$f_i \approx \frac{75}{10.283 a_i \sqrt{\varepsilon_{eff}}} \tag{2}$$

A Rogers RO4350B is embedded into the FR4 to create the CT and which is the proposed antenna configuration. Unlike the traditional multilayer substrate, the proposed countersink technique can be seen as a particular case of multilayer configuration involving two inhomogeneous materials. Therefore, the two-layer dielectric can be modeled using each substrate layer's effective permittivity and simplified into a single equivalent homogeneous substrate with a thickness of h_{eq} and the dielectric constant ε_{eff}, as illustrated in Figure 2.

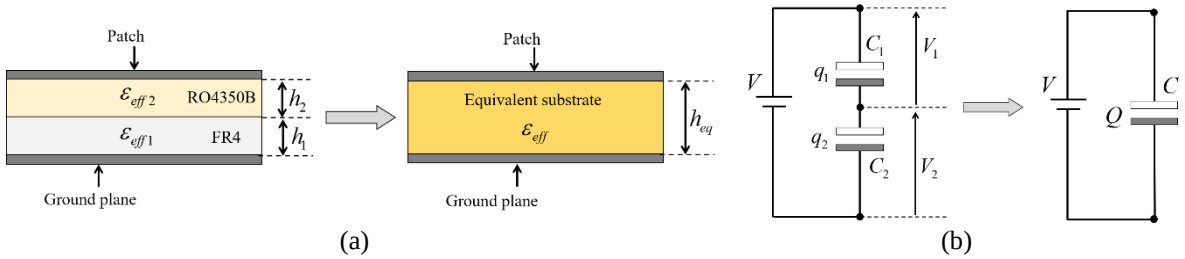

Figure 2 Simplification of the two-layer substrate into a single layer through parallel plate capacitor. (a) model; (b) circuit

By using the parallel plate capacitor model presented, the equivalent capacitance C per unit area can be computed in terms of the electric charge Q per unit area and the electric potential difference V between two plates [27]

$$C = \frac{Q}{V} = \frac{1}{\left(\frac{1}{\varepsilon_{eff}}\right) h_{eq}} \tag{3}$$

Received: Added at production | Revised: Added at production | Accepted: Added at production
DOI: xxx/xxxx

The dielectric constant ε_{eff} and the height h_{eq} of the equivalent substrate in equation (3) can be expressed by [28].

$$\varepsilon_{eff} = h_{eq}\left[\sum_{n=1}^{2}\left(\frac{h_n}{\varepsilon_{effn}}\right)\right]^{-1} \tag{4}$$

$$h_{eq} = \sum_{n}^{2} h_n = h_1 + h_2 \tag{5}$$

Expanding equation (4) and using equation (5) yields

$$\varepsilon_{eff} \approx \frac{\varepsilon_{eff1}\varepsilon_{eff2}\left(h_1 + h_2\right)}{h_2\varepsilon_{eff1} + h_1\varepsilon_{eff2}} \tag{6}$$

where the effective permittivity for each layer can be approximated as

$$\varepsilon_{eff1} \approx \frac{\varepsilon_{r1} + 1}{2} \tag{7}$$

$$\varepsilon_{eff2} \approx \frac{\varepsilon_{r2} + 1}{2} \tag{8}$$

Using the Equations (2), (6)-(8), the three resonant frequencies of the triband are 2.74 GHz, 3.62 GHz, and 4.43 GHz.

To analyze the developed mathematical model for the proposed antenna structure, Maxwell's equations through an electromagnetic software were used to evaluate and compare the resonant frequencies obtained analytically from Equation (2), which mainly depends on the different current path lengths of each heart-shaped branch. To further characterize the antenna design, a parametric study of the circular part radius "*a*" of the radiating element is carried out. To facilitate the parametric analysis, every path's circular part radius is expressed in terms of the primary radius "*a*" and given by

$$a_i = \frac{a}{0.4\left(i+2\right)},\ i=1,2,3. \tag{9}$$

It can be observed from the plots in Figure 3 that by increasing "*a*", the resonant frequencies shift downward. Similarly, the resonant frequencies of the presented antenna increase when the size of the antenna reduces.

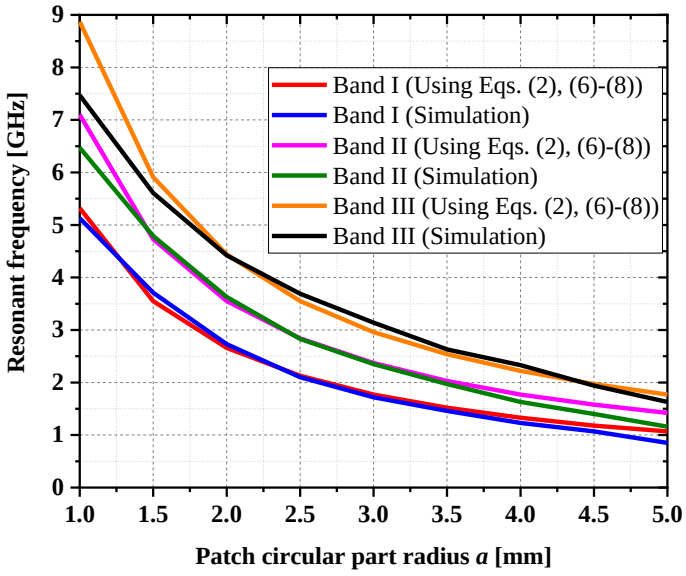

Received: Added at production | Revised: Added at production | Accepted: Added at production
DOI: xxx/xxxx

Figure 3 Parametric analysis of the proposed antenna

Figure 3 illustrates that by varying the antenna structure dimensions and using Equations (2), (6)-(8), the analytical and simulated results agree for the three frequency bands. This validates the developed mathematical model for the proposed heart-shaped planar monopole antenna.

3 | RESULTS AND DISCUSSION

3.1 | COUNTERSINK TECHNIQUE EFFECT

Two triband heart-shaped planar monopole antennas with and without the embedded substrate are analyzed to evaluate the effect countersink technique on the antenna performance. The return loss simulation results through an electromagnetic simulator are displayed in Figure 4 below.

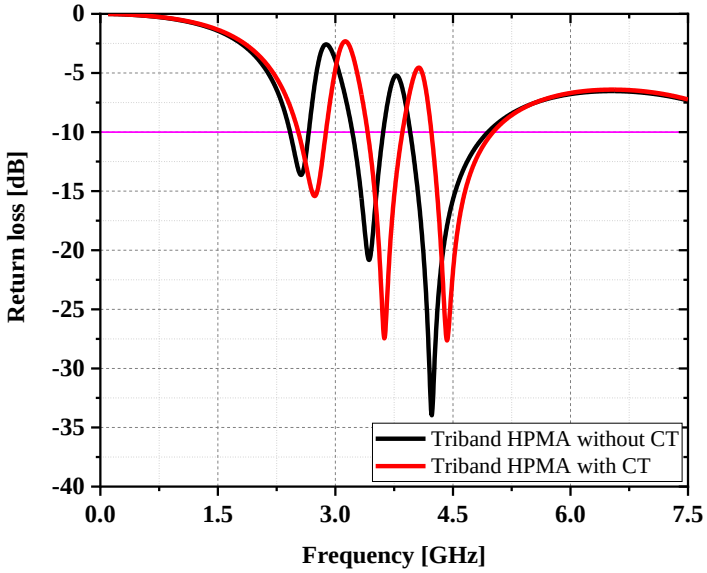

Figure 4 Simulated return loss comparison

Figure 4 demonstrates that the proposed antenna is well much across all the frequency bands compared to the same antenna configuration without CT. The other performance parameters for the two antenna configurations are presented in Table 2.

Table 2 Simulation results comparison for two HPMA configurations

Antenna parameter	Antenna configuration					
	Triband HPMA without CT			Triband HPMA with CT		
	Band I	Band II	Band III	Band I	Band II	Band III
Resonant frequency (GHz)	2.56	3.43	4.23	2.74	3.62	4.43
Return Loss (dB)	-13.63	-20.79	-33.96	-15.41	-27.46	-27.59
Bandwidth (MHz) (S_{11}≤ -10 dB)	236	388.6	989.7	347	439.4	786.3
Radiation efficiency (%)	41.16	52.47	60.55	57.8	71.26	40.16
Gain (dB)	-2.1	-0.6	-0.2	-0.7	0.4	-2.1
VSWR	1.528	1.201	1.041	1.398	1.095	1.091

From Table 2, it can be observed that except in (Band III), embedding the Rogers RO4350B into FR4 and employing slits along with DGS yield better antenna performance results in the first (Band I) and second (Band II) operating frequency bands. It is observed an offset of about 100 MHz between the resonant frequencies for the two antenna configurations. This shift increases by 100 MHz at each resonance frequency within each band. Moreover, the triband HPMA with CT achieves a better matching level through the return loss with a slight difference of resonant frequency for the third band (Band III). It is also noticed that apart from the first and the second frequency bands, the triband HPMA without CT yields wider bandwidth and radiation efficiency in the third band. However, parameters like antenna gain and radiation efficiency are better when the countersink

Received: Added at production | Revised: Added at production | Accepted: Added at production
DOI: xxx/xxxx

technique is used. Finally, the HPMA using the countersink technique seems to be a promising way to improve an antenna's performance regarding the results obtained by electromagnetic simulations.

3.2 | ANTENNA RETURN LOSS

From the results detailed above, an HPMA prototype in the countersink technique has been manufactured. Figure 5 displays the HPMA prototype fabricated using the countersink technique with the two insulators: RO4350B thermally embedded into FR4 HTG175.

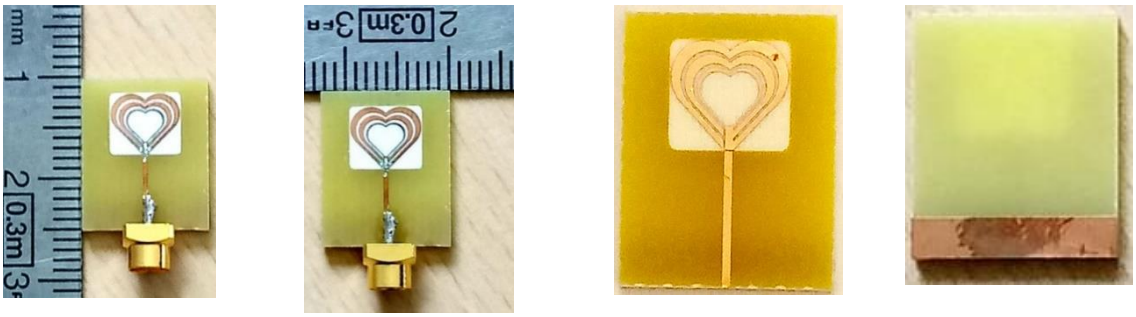

(a) (b) (c) (d)

Figure 5 Photograph of the fabricated antenna prototype using countersink technique. (a, b, c) to view; (d) bottom view

The simulated and measured return loss curves for the HPMA are presented in Figure 6. From the measured frequency response, it can be observed that for $|S_{11}| \leq -10$ dB, the antenna can operate over the bands (2.695 – 2.89 GHz), (3.51 – 3.77 GHz), and (4.92 – 5.46 GHz). The first band is suitable for weather and airport surveillance radars operating in the 2.7–2.9 GHz range; the second band coverage includes LTE bands 42/43/48, 5G, WiMAX applications, and in the third band, 5 GHz WLAN (5.15 – 5.35 GHz) and UNII Low UNII – 2A/2B (5.15 – 5.47 GHz) applications are covered.

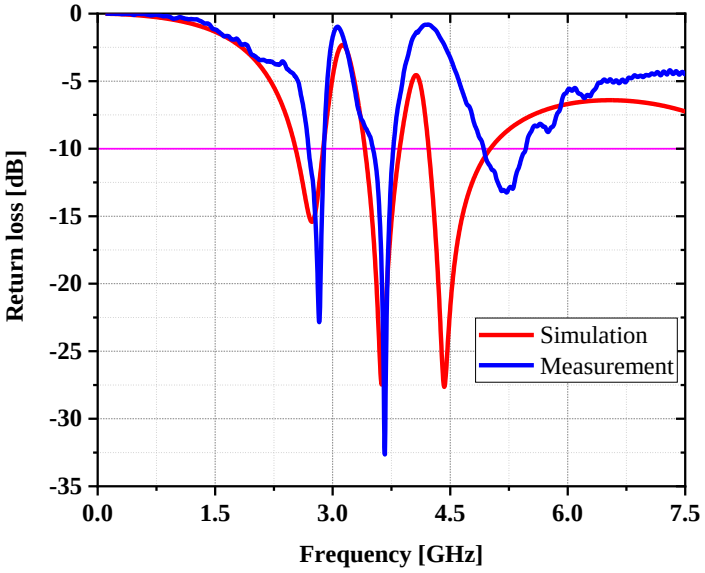

Figure 6 Return loss of the proposed antenna

At -10 dB of the return loss parameter, the HPMA guarantees 195 MHz of bandwidth. Furthermore, the experimental results demonstrate that the use of slits and the partial ground plane yielded significant antenna miniaturization. The antenna size reduction has been evaluated using two approaches. The first approach compares the active patch area of a typical microstrip antenna resonating at the same frequency with the proposed antenna active patch area as given in Equation (10).

Received: Added at production | Revised: Added at production | Accepted: Added at production
DOI: xxx/xxxx

$$M(\%) = \left[\frac{A_r(f_r)\big|_{(f_r=f_0)} - A_p(f_r)\big|_{(f_r=f_0)}}{A_r(f_r)\big|_{(f_r=f_0)}} \right] \times 100 \tag{10}$$

where A_r is the active patch area of a typical microstrip antenna (rectangular patch, circular patch, elliptical patch) resonating at the same resonant frequency f_0 with the proposed antenna having an active patch area of A_p.

A typical rectangular microstrip antenna resonating at 2.83 GHz has a minimum active patch area of 801.78 mm^2 (24.9 mm × 32.2 mm). In contrast, a standard circular microstrip patch antenna resonating at the same frequency (2.83 GHz) has a radius of 14.34 mm with a minimum active patch area of 646 mm^2. Comparing the proposed HPMA to the typical rectangular and circular microstrip patch antennas mentioned above through the Equation (10) yields a significant antenna's active patch size reduction of about 96.4 % and 95.6 %, respectively.

The proposed design structure is simulated with and without slits and a partial ground plane to quantify the antenna miniaturization in the second and final approach. The results are compared in terms of the lower resonant frequency, as shown in Figure 7. As it can be observed, the conventional heart-shaped antenna resonates at 13.42 GHz, while the proposed antenna's lower resonant frequency is 2.74 GHz.

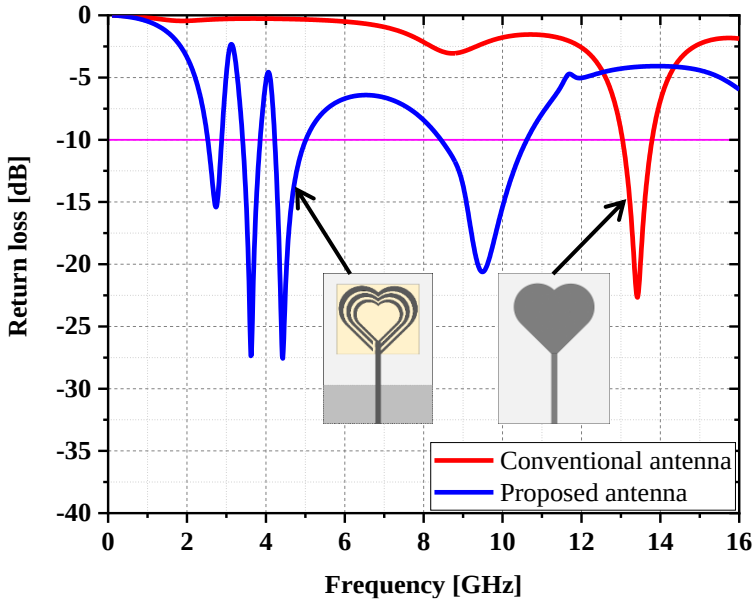

Figure 7 Comparison between the conventional antenna and the proposed

This clearly illustrates that truncating the ground plane and etching slits on the radiating element after embedding the rogers RO4350B into FR4 yields a 79.58% reduction in resonant frequency, which can be computed using the following formula:

$$M(\%) = \left[\frac{f_{r0} - f_{r1}}{f_{r0}} \right] \times 100 \tag{11}$$

where f_{r0} is the lower resonant frequency of the conventional planar heart-shaped antenna and f_{r1}, the lower resonant frequency of the proposed antenna design based on countersink technique and partial ground plane along with open-ended multiple branches through slits.

The simulated and experimental results presented in Figure 8 indicate that the HPMA has good matching with a Voltage Standing Wave Ratio (VSWR) values less than 1.56 at all its respective resonant frequencies. This points out a good matching between the feed network and the antenna structure.

Received: Added at production | Revised: Added at production | Accepted: Added at production
DOI: xxx/xxxx

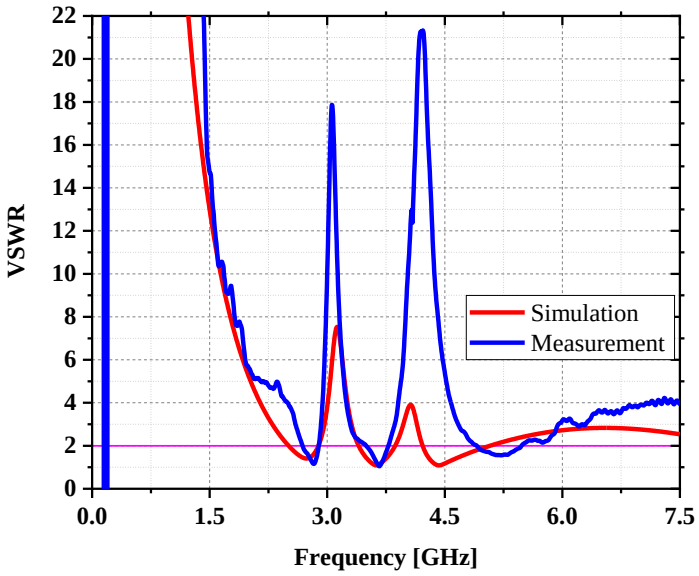

Figure 8 Antenna simulated and measured VSWR

3.3 | SURFACE CURRENT DISTRIBUTION

Figure 9 illustrates the radiating element's surface current distributions at 2.74 GHz, 3.62 GHz, and 4.43 GHz, with a maximum intensity of 82.3 A/m, 111.6 A/m, and 402.7 A/m, respectively.

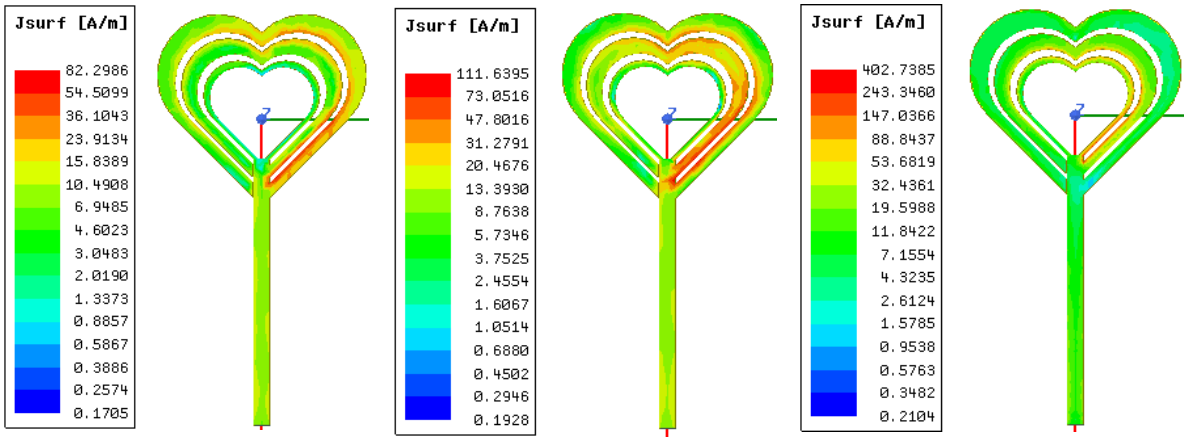

(a) (b) (c)

Figure 9 Simulated surface current distribution. (a) 2.74 GHz; (b) 3.62 GHz; (c) 4.43 GHz

It can be well noticed from Figure 9 (a) that at 2.74 GHz, maximum current is strongly concentrated around the first open-ended heart-shaped slit followed by the edges of the radiating element. This confirms that that slit generates the first frequency band. In contrast, a nearly uniform current is distributed on the other part of the antenna patch surface. At 3.62 GHz, most of the surface current is distributed around the first open-ended slit and the second open-ended branch, as shown in Figure 9 (b). Hence, the middle resonant frequency can be mainly controlled by the second heart-shaped open-ended branch. The other parts of the radiating element exhibit similar behavior to that of 2.74 GHz. Lastly, from Figure 9 (c), it is observed that at 4.43 GHz, the intensity of radiation current is more concentrated around the second open-ended slit and in the inner strip. It is evident that the third resonance can be controlled with the inner heart-shaped strip.

Received: Added at production | Revised: Added at production | Accepted: Added at production
DOI: xxx/xxxx

3.4 | RADIATION PATTERN OF THE HPMA

The antenna radiated field consists of near-field and far-field regions from the antenna. For this work, the far-field radiation pattern measurement has been conducted in an anechoic chamber in the presence of a horn receiving antenna as a reference device. The results are presented in Figure 10. The antenna exhibits an omnidirectional radiation pattern in the elevation plane, and a deviating quasi-bidirectional pattern in the azimuth plane in the entire operating frequency range with maximum radiation in the azimuth plane found at ϕ=0º. This satisfies the radiation performance characteristics of monopole antennas.

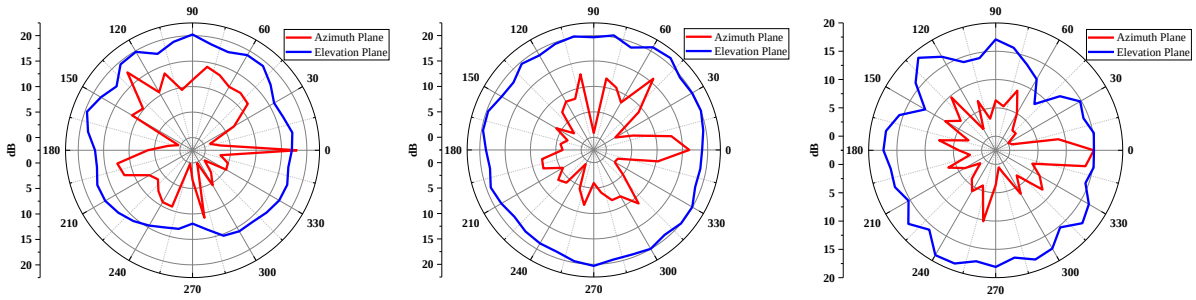

Figure 10 Antenna measured radiation pattern. (a) 2.83 GHz; (b) 3.67 GHz; (c) 5.22 GHz

The simulated antenna efficiency against frequency for the proposed antenna across the three bands is shown in Figure 11. It can be observed a radiation efficiency of about 57.8 %, 71.26 %, and 40.16 % obtained at 2.74 GHz, 3.62 GHz, and 4.43 GHz, respectively.

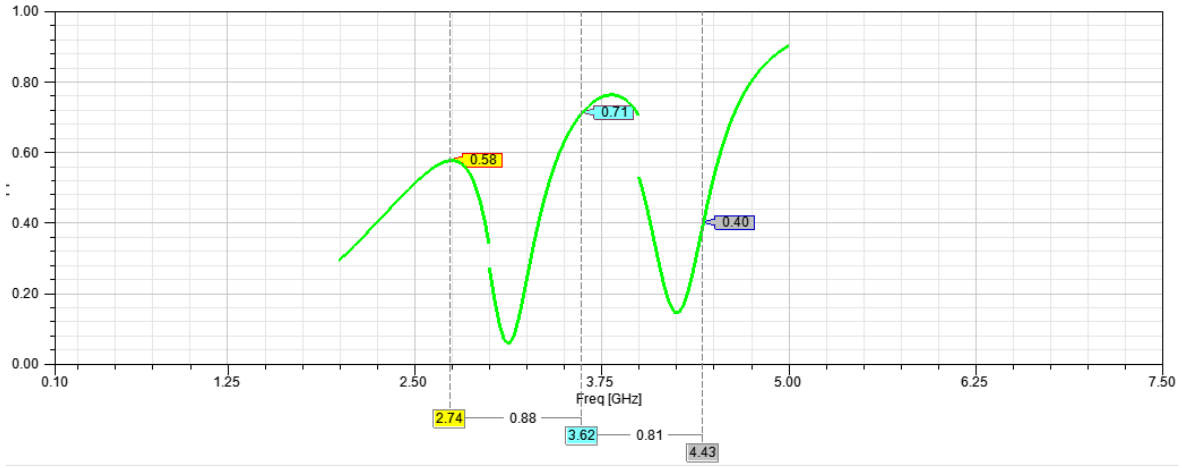

Figure 11. Simulated efficiency versus frequency of the proposed antenna

3.5 | GAIN OF THE HPMA

The antenna gain is one of the essential parameters that predicts its effective transmission or reception ability. The antenna gain is determined from the *Two - Antenna Method* [29] based on the Friis' formula given below

$$\left|S_{21}\right|^2 = G_t G_{ref} \left(\frac{c}{4\pi d f_0}\right)^2 \tag{12}$$

where d is the distance between both antennas, G_t and G_{ref} the gain of the transmitting and receiving antenna, f_0 the operating frequency, and S_{21} the transmission coefficient between both antennas. Using two identical antennas and applying the Friis principle, Equation (12) becomes in decibel as:

Received: Added at production | Revised: Added at production | Accepted: Added at production
DOI: xxx/xxxx

$$G_t^{dBi} = \frac{1}{2}\left[S_{21}^{dB} + 32.5 + 20\log\left(f_{0_{(GHz)}} \right) + 20\log\left(d_{(m)} \right) \right] \quad (13)$$

By placing the transmitting and receiving antennas at a distance d=135 mm from each other and using Equation (13), the measured results show that the proposed antenna achieves a maximum gain of 0.18 dBi at 3.78 GHz, whereas 0.56 dBi maximum gain is found at 3.76 GHz from the simulation.

The simulated antenna gain is displayed in Figure 12 below. At the first resonant frequency (2.74 GHz), the simulated gain is about -0.7 dB. For the medium band, the simulated antenna gain is about 0.4 dB at 3.62 GHz, and at 4.43 GHz, the simulated gain is -2.1 dB for the higher band of operation.

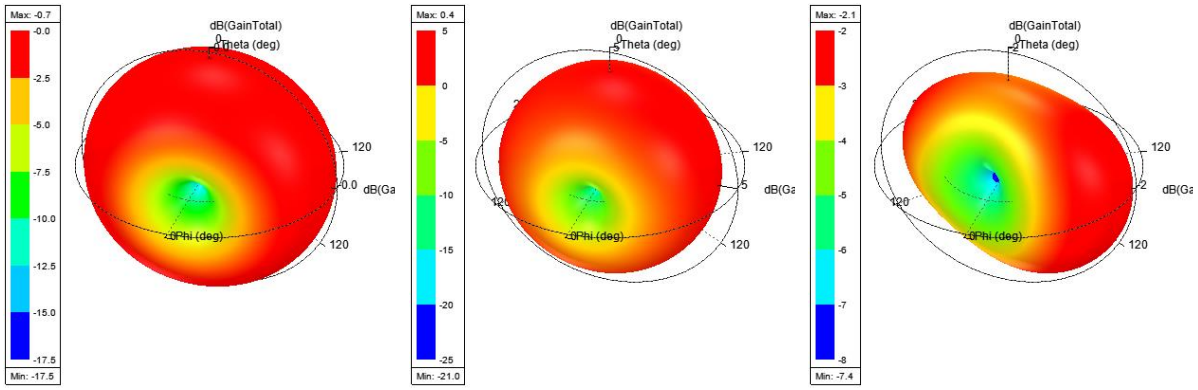

(a) (b) (c)

Figure 12 Simulated gain. (a) 2.74 GHz; (b) 3.62 GHz; (c) 4.43 GHz

When miniaturizing an antenna, its gain, radiation efficiency, bandwidth, and polarization purity are affected [30]. Moreover, an Electrically Small Antenna [31] can have a negative gain, even lower than -10 dB, without accounting for impedance mismatch loss [32]. This follows directly from the fact that using DGS in the HPMA is responsible for low radiated power that yielded low antenna gains and efficiencies. Table 3 summarizes the simulated and experimental results for the HPMA.

Table 3 Simulation and experimental results comparison for the HPMA

Results		**Band I**	**Band II**	**Band III**
Simulation	***f_r (GHz)***	2.74	3.62	4.43
	S_{11} (dB)	-15.41	-27.46	-27.59
	Bandwidth (MHz)	347	439.4	786.3
	Efficiency (%)	57.8	71.26	40.16
	Gain (dB)	-0.7	0.4	-2.1
Measurement	***f_r (GHz)***	2.83	3.66	5.21
	S_{11} (dB)	-22.84	-32.65	-13.25
	Bandwidth (MHz)	195	260	530
	Gain (dBi)	-0.77	-0.84	-2.48

It can be observed that the antenna performs as a narrowband in its lower and middle operating frequency bands and exhibits wideband behavior in its upper bands with a minimum bandwidth of 500 MHz. The proposed antennas find their application in mobile phones and consumer electronics products whose efficiency range is 20% - 70% [33]. Table 4 compares the performance of the proposed antenna to the other existing antennas in the literature.

Received: Added at production | Revised: Added at production | Accepted: Added at production
DOI: xxx/xxxx

Table 4 Comparison with previously reported antennas

Ref.	Electrical size	Physical size (mm)	Patch area (mm^2)	Substrate	Method	Application
[34]	$0.176\lambda_0 \times 0.144\lambda_0 \times 0.008\lambda_0$	18×22×1	195.75	FR4	Multiple branches and DGS	WLAN, WiMAX, X-band application
[35]	$0.150\lambda_0 \times 0.150\lambda_0 \times 0.016\lambda_0$	15×15×1.6	105	FR4	Slots/Slits and DGS	WLAN, WiMAX, ITU
[36]	$0.220\lambda_0 \times 0.258 \times 0.006\lambda_0$	34×29×0.8	238	FR4	Slits and DGS	WLAN, WiMAX
[37]	$0.193\lambda_0 \times 0.204\lambda_0 \times 0.009\lambda_0$	17×18×0.8	100.53	FR4	Slots and DGS	WLAN, WiMAX
[38]	$0.235\lambda_0 \times 0.267\lambda_0 \times 0.013\lambda_0$	30×34×1.6	520	FR4	DGS	WLAN, WiMAX
[39]	$0.417\lambda_0 \times 0.292\lambda_0 \times 0.0133\lambda_0$	50×35×1.6	93.5	FR4	DGS, L- and U-shaped strip-loaded	WLAN, WiMAX
HPMA	$0.127\lambda_0 \times 0.105\lambda_0 \times 0.013\lambda_0$	15×12.5×1.524	28.5	FR4+RO 4350B	Open-ended multiple branches, DGS, and countersink technique	WLAN, WiMAX, LTE, 5G, UNII, Weather radars, Airport surveillance radars

As it can be read from Table 3, the HPMA can be used in more than three applications. Also, with a physical size of 15×12.5×1.524 mm^3 and an electrical size of $0.127\lambda_0 \times 0.105\lambda_0 \times 0.013\lambda_0$ at its lowest operating frequency (2.53GHz), this HPMA is the smallest antenna device compared to the other triband designs.

4 | CONCLUSION

In this paper, a new configuration of a miniaturized triband heart-shaped planar monopole antenna (HPMA) has been investigated. The antenna design is based on the countersink technique (CT) to improve certain specific electromagnetic performance parameters with microstrip technology. A mathematical model has been developed to predict the resonant frequencies of the proposed antenna structure configuration. Furthermore, the HPMA, proposed with further details, guarantees a minimum bandwidth of 195 MHz and achieves wideband operation in its upper band. The embedded substrate plays a key role in improving antenna performance without increasing the antenna surface area or the structure volume. In contrast, the defected ground structure and slits resulted in a 79.58% reduction in resonant frequency while preserving the fidelity of other performance parameters within an acceptable range for the targeted wireless applications. The measurement results demonstrate that the proposed HPMA achieves a minimum return loss of -32.65 dB and a maximum of -13.25 dB. The countersink technique complexity makes the structure challenging to manufacture, yielding high fabrication costs. Its measured and computer-simulated results well-agreed in the operating frequency range. The proposed antenna configuration covers WLAN, WiMAX, LTE, 5G, UNII, Weather radars, and Airport surveillance radars applications. Besides its simple design methodology, the HPMA is compact and meets the requirement of 2:1 VSWR, which are the key features that make it a potential candidate for handheld wireless devices.

ACKNOWLEDGEMENTS

Grateful acknowledgement is made to the African Union Commission for sponsoring the research through the Pan African University Institute for Basic Sciences Technology and Innovation (PAUSTI). Also, the authors give special thanks to Pheline Laboratory for great help during the validation process of the antenna prototypes.

REFERENCES

1. 5G - Fifth generation of mobile technologies. Published 2019. Accessed December 10, 2020.

https://www.itu.int/en/mediacentre/backgrounders/Pages/5G-fifth-generation-of-mobile-technologies.aspx

2. Zhi R, Han M, Bai J, Wu W, Liu G. Miniature multiband antenna for WLAN and X-Band satellite communication applications. *Prog Electromagn Res Lett*. 2018;13-18. https://doi.org/10.2528/pierl18021805
3. Bag B, Biswas P, Mondal R, Biswas S, Sarkar PP. Circularly polarized quad-band monopole antenna of wireless communication system. *Int J RF Microw Comput Eng*. 2019;e21818. https://doi.org/10.1002/mmce.21818
4. Sharawi MS, Khan MU, Mittra R. Microstrip patch antenna miniaturisation techniques: a review. *IET Microwaves, Antennas Propag*. 2015;913-922. https://doi.org/10.1049/iet-map.2014.0602
5. Patel R, Upadhyaya T, Desai A, Palandoken M. Low Profile Multiband Meander Antenna for LTE/WiMAX/WLAN and INSAT-C Application. *AEU - Int J Electron Commun*. 2019;90-98. https://doi.org/10.1016/j.aeue.2019.02.010
6. Chetouah F, Aidel S, Bouzit N, Messaoudene I. A miniaturized printed monopole antenna for 5.2-5.8 GHz WLAN applications. *Int J RF Microw Comput Eng*. 2018;e21250. https://doi.org/10.1002/mmce.21250
7. Ambh A, Singhal PK. Size Reduction of Rectangular Microstrip Patch Microstrip Antenna for GSM Application. *Int Res J Eng Technol*. 2016;255-258.
8. Li Y, Yu W. A Miniaturized Triple Band Monopole Antenna for WLAN and WiMAX Applications. *Int J Antennas Propag*. 2015. https://doi.org/10.1155/2015/146780
9. Kumar Y, Gangwar RK, Kanaujia BK. Compact broadband circularly polarized Hook-shaped microstrip antenna with DGS plane. *Int J RF Microw Comput Eng*. 2018;e21275. https://doi.org/10.1002/mmce.21275
10. Wu BJ, Feng QY. A novel compact broadband antenna for LTE/WLAN/WiMAX applications. *Prog Electromagn Res Lett*. 2016;129-135. https://doi.org/10.2528/PIERL16030403
11. Verma MK, Kanaujia BK, Saini JP, Singh P. A compact multi-slots loaded gap coupled CP antenna with DGS for WLAN/WiMAX applications. *Int J RF Microw Comput Eng*. 2020;e22431. https://doi.org/10.1002/mmce.22431
12. Chen Z, Lu B, Zhu Y, Lv H. A Compact Printed Monopole Antenna for WiMAX/WLAN and UWB Applications. *Futur Internet*. 2018;122. https://doi.org/10.3390/fi10120122
13. Sah BK, Singla G, Sharma S. Design and development of enhanced bandwidth multi-frequency slotted antenna for 4G-LTE/WiMAX/WLAN and S/C/X-band applications. *Int J RF Microw Comput Eng*. 2020;e22214. https://doi.org/10.1002/mmce.22214
14. Ahmad H, Zaman W, Bashir S, Rahman MU. Compact triband slotted printed monopole antenna for WLAN and WiMAX applications. *Int J RF Microw Comput Eng*. 2020;e21986. https://doi.org/10.1002/mmce.21986
15. Rothwell EJ, Ouedraogo RO. Antenna miniaturization: definitions, concepts, and a review with emphasis on metamaterials. *J Electromagn Waves Appl*. 2014;2089-2123. https://doi.org/10.1080/09205071.2014.972470
16. Asif S, Iftikhar A, Rafiq MN, et al. A compact multiband microstrip patch antenna with U-shaped parasitic elements. *IEEE Antennas Propag Soc AP-S Int Symp*. 2015;617-618. https://doi.org/10.1109/APS.2015.7304695
17. Faisal GM, Alqaisy MA. Multi-Band Microstrip Antenna Design for Mobile Phone Applications. *2017 2nd Al-Sadiq Int Conf Multidiscip IT Commun Sci Appl AIC-MITCSA 2017*. Published online 2019;287-290. https://doi.org/10.1109/AIC-MITCSA.2017.8723008
18. Akinola S, Hashimu I, Singh G. Gain and Bandwidth Enhancement Techniques of Microstrip Antenna: A Technical Review. *Proc 2019 Int Conf Comput Intell Knowl Econ ICCIKE 2019*. 2019;175-180. https://doi.org/10.1109/ICCIKE47802.2019.9004278
19. Agale T, Khanapurkar MM. A review on design approach for performance enhancement techniques of microstrip patch antenna. *Proc 3rd IEEE Int Conf Adv Electr Electron Information, Commun Bio-Informatics, AEEICB 2017*. Published online 2017;436-440. https://doi.org/10.1109/AEEICB.2017.7972348
20. Moukala Mpele P, Moukanda Mbango F, Onyango Konditi DB. A Small Dual Band (28/38 GHz) Elliptical Antenna For 5G Applications With DGS. *Int J Sci Technol Res*. 2019;353-357.
21. Darimireddy NK, Ramana Reddy R, Mallikarjuna Prasad A. Design of triple-layer double U-slot patch antenna for wireless applications. *J Appl Res Technol*. 2015;526-534. https://doi.org/10.1016/j.jart.2015.10.006
22. Gustafsson M, Capek M, Schab K. Tradeoff between Antenna Efficiency and Q-Factor. *IEEE Trans*

Antennas Propag. 2019;2482-2493. https://doi.org/10.1109/TAP.2019.2891448

23. Prasad Rao R, Srinu B, Dharma Raj C. Design and analysis of multi substrate microstrip patch antenna. *Lect Notes Electr Eng*. 2016;733-739. https://doi.org/10.1007/978-81-322-2728-1_70
24. Kim JH, Hyeon CK, Chun K. Performance enhancements of a microstrip antenna with multiple layer substrates. *Conf Proc Int Symp Signals, Syst Electron*. Published online 2007;319-322. https://doi.org/10.1109/ISSSE.2007.4294477
25. Ineneji CN, Kusaf M. Gain enhancement in microstrip patch antenna using the Multiple Substrate Layer method. *2015 23rd Signal Process Commun Appl Conf SIU 2015 - Proc*. Published online 2015;560. https://doi.org/10.1109/SIU.2015.7129885
26. Zehforoosh Y, Ghobadi C, Nourinia J. Antenna Design for Ultra Wideband Application Using a New Multilayer Structure. *PIERS Online*. 2006;544-549. https://doi.org/10.2529/piers060531145356
27. Hu F, Song J, Kamgaing T. Modeling of multilayered media using effective medium theory. In: *19th Topical Meeting on Electrical Performance of Electronic Packaging and Systems*. Vol 1. IEEE; 2010:225-228. https://doi.org/10.1109/EPEPS.2010.5642584
28. Ali WKW, Al-Charchafchi SH. Using equivalent dielectric constant to simplify the analysis of patch microstrip antenna with multi-layer substrates. *IEEE Antennas Propag Soc Int Symp 1998 Dig - Antennas Gateways to Glob Netw - Held conjunction with Usn Natl Radio Sci Meet*. 1998;676-679. https://doi.org/10.1109/APS.1998.702028
29. Balanis CA. *Antenna Theory : Analysis and Design*. 4th ed. Wiley; 2016.
30. Skrivervik AK, Zürcher JF, Staub O, Mosig JR. PCS antenna design: The challenge of miniaturization. *IEEE Antennas Propag Mag*. 2001;12-27. https://doi.org/10.1109/74.951556
31. Fujimoto K (Kyōhei), Ito K. *Antennas for Small Mobile Terminals*. 2nd ed. Artech House; 2018.
32. Antenna Gain. Published 2016. Accessed February 3, 2020. http://www.antenna-theory.com/basics/gain.php
33. Antenna Efficiency. Published 2016. Accessed October 22, 2020. http://www.antenna-theory.com/basics/efficiency.php
34. Liu T, Sun Y, Li J, Yu J, Wang K. CPW-fed compact multiband monopole antenna for WLAN/WiMAX/X-band application. *Prog Electromagn Res Lett*. 2019;105-113. https://doi.org/10.2528/pierl19080902
35. Rezvani M, Zehforoosh Y. Design of Multi-band Microstrip Antenna for Wireless Communications and ITU Applications. *Natl Acad Sci Lett*. 2017;331-334. https://doi.org/10.1007/s40009-017-0574-1
36. Chandan, Srivastava T, Rai BS. L-Slotted Microstrip Fed Monopole Antenna for Triple Band WLAN and WiMAX Applications. In: *Proceedings of the 5th International Conference on Frontiers in Intelligent Computing: Theory and Applications, Advances in Intelligent Systems and Computing*. ; 2017:351-359. https://doi.org/10.1007/978-981-10-3156-4_36
37. Naji DK. Miniature slotted semi-circular dual-band antenna for WiMAX and WLAN applications. *J Electromagn Eng Sci*. 2020;115-124. https://doi.org/10.26866/JEES.2020.20.2.115
38. Ibrahim A, Arina Fazil N, Dewan R. Triple-band antenna with defected ground structure (DGS) for WLAN/WiMAX applications. *J Phys Conf Ser*. 2020;012071. https://doi.org/10.1088/1742-6596/1432/1/012071
39. Bag B, Biswas P, Mondal R, Biswas S, Sarkar PP. Dual-band dual-sense circularly polarized U- and L-shaped strip monopole antenna for WiMAX/WLAN applications. *J Electromagn Waves Appl*. 2019;2434-2448. https://doi.org/10.1080/09205071.2019.1684387

AUTHOR BIOGRAPHIES

Pierre Moukala Mpele was born in 1990, in Makoungou (Republic of Congo). He received the B.S and M.S degrees in Electronics and Telecommunication from the National School of Polytechnic Studies, Marien Ngouabi University, Brazzaville (Congo) in 2013 and 2016, respectively. He is currently pursuing the Ph.D. degree in Electrical engineering, specialized in Telecommunication at Pan African University Institute for Basic Science Technology and Innovation (PAUSTI), Juja-Nairobi, Kenya. His research interests include microstrip antennas miniaturization, wireless communication systems, networking, and cybersecurity.

Received: Added at production | Revised: Added at production | Accepted: Added at production
DOI: xxx/xxxx

Franck Moukanda Mbango was born in 1973 in Pointe-Noire (Republic of Congo) and received an Engineer degree in microwave electronics from Mouloud Mammeri University (Algeria) in 2001. In 2003 and 2008, he respectively received the M.Sc and the Ph.D. degrees in microwave circuits from National Polytechnic Institute (INP) and Joseph FOURIER University at Grenoble, France. From 2009 to 2014, he was involved in several telecommunications industrial projects as an R&D Engineer and Research Assistant Consultant to ALTRAN Technologies for Vallourec and Electromagnetic Compatibility (EMC) Engineer to Scientific and Technical Center for Building (CSTB). He currently works as CAMES Senior Lecturer and researcher at Marien Ngouabi University, Congo Republic, and a part-time teacher at Pan African University Institute for Basic Sciences Technology and Innovation (PAUISTI), Kenya. His research fields focus on high-frequency material measurement techniques, microwave device Electromagnetic modeling for wireless applications, electromagnetic environment impact, and microwave design (planar antennas and circuits: filters, power dividers, etc.) systems.

Dominic Bernard Onyango Konditi was born in Kochia, Homa-Bay County, in 1950. He is a professor of Electrical and Electronic Engineering, Director of Open and Lifelong Education, and former Director of School of Electrical & Electronic Engineering at The Technical University of Kenya. He holds a Ph.D. in Electronics and Computer Engineering from the Indian Institute of Technology Roorkee and an MSc-Eng. in Electrical Engineering from Tottori University, JAPAN, Postgrad Res. from Dresden University of Technology (Germany), and Higher National Diploma in Electrical Engineering from Mombasa Polytechnic. His research interests are in Advanced Antenna Systems and Design, EMC/EMI Problems, Computational Electromagnetics, and Microwave Engineering.

Fabien Ndagijimana is Professor at Université Grenoble Alpes in Grenoble-France. He received his Ph.D., specializing in Microwave and optoelectronics, in December 1990, at Institut National Polytechnique de Grenoble (INPG) in France. He then joined the faculty of Electrical Engineering ENSERG as Associate Professor, where he teaches microwave techniques and electromagnetic modeling. Since September 1997, he joined the Université Grenoble Alpes, where he is a full professor at the Institut Universitaire de Technologie (IUT). His research activity focuses on the characterization and electromagnetic modeling of microwave devices for wireless applications, signal integrity in high-speed applications, and test tools for electromagnetic compatibility standards.